JACS
JOURNAL OF THE AMERICAN CHEMICAL SOCIETY

Article

pubs.acs.org/JACS

Nanoscale Structure–Activity Relationships, Mode of Action, and Biocompatibility of Gold Nanoparticle Antibiotics

Jamee Bresee,[†] Constance M. Bond,[‡] Roberta J. Worthington,[‡] Candice A. Smith,[†] Jennifer C. Gifford,[†] Carrie A. Simpson,[†] Carly J. Carter,[†] Guankui Wang,[†] Jesse Hartman,[†] Niki A. Osbaugh,[†] Richard K. Shoemaker,[†] Christian Melander,*[,‡] and Daniel L. Feldheim*[,†]

[†]Department of Chemistry and Biochemistry, University of Colorado, Boulder, Colorado 80309, United States

[‡]Department of Chemistry, North Carolina State University, Raleigh, North Carolina 27695, United States

Supporting Information

ABSTRACT: The emergence of resistance to multiple antimicrobial agents by pathogenic bacteria has become a significant global public health threat. Multi-drug-resistant (MDR) Gram-negative bacteria have become particularly problematic, as no new classes of small-molecule antibiotics for Gram-negative bacteria have emerged in over two decades. We have developed a combinatorial screening process for identifying mixed ligand monolayer/gold nanoparticle conjugates (2.4 nm diameter) with antibiotic activity. The method previously led to the discovery of several conjugates with potent activity against the Gram-negative bacterium *Escherichia coli*. Here we show that these conjugates are also active against MDR *E. coli* and MDR *Klebsiella pneumoniae*. Moreover, we have shown that resistance to these nanoparticles develops significantly more slowly than to a commercial small-molecule drug. These results, combined with their relatively low toxicity to mammalian cells and biocompatibility in vivo, suggest that gold nanoparticles may be viable new candidates for the treatment of MDR Gram-negative bacterial infections.

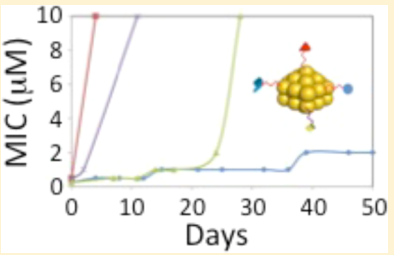

INTRODUCTION

The emergence of resistance to multiple antimicrobial agents in pathogenic bacteria has become a significant global public health threat. Drug-resistant bacterial infections cause considerable patient mortality and morbidity, and rising antibiotic resistance is seriously threatening the vast medical advancements made possible by antibiotics over the past 70 years. Without developing innovative approaches to combat these multi-drug-resistant (MDR) pathogens, many fields of medicine will be severely affected, including surgery, premature infant care, cancer chemotherapy, care of the critically ill, and transplantation medicine, all of which are feasible only with the existence of effective antibiotic therapy. This situation is so dire that the World Health Organization has identified MDR bacteria as one of the top three threats to human health,[1] while the Infectious Disease Society of America has issued a call to action from the biomedical community to deal with the MDR bacterial threat.[2]

In response to this unmet medical need, our laboratories and others have been exploring synthetic ligand-coated gold nanoparticles (1–5 nm diameter) as therapeutics for the treatment of viral and bacterial diseases.[3−6] Gold nanoparticle therapeutics have a number of unique properties that are distinct from small-molecule therapeutics including tunable valency and in vivo circulation half-life, diameters that are slightly larger than drug efflux pumps, and the ability to disrupt protein–protein interactions.[7−11] These characteristics suggest that gold nanoparticles may have the potential to access new pathogen targets and delay the onset of drug resistance.

Another important characteristic of gold nanoparticles is the ease with which they can be synthesized and modified with one or more chemically distinct thiol ligands.[12−14] We showed previously that this thiol modification chemistry enables the rapid construction of combinatorial libraries of small-molecule/gold nanoparticle conjugates that may be screened for biological activity.[4,5] In this small-molecule variable ligand display (SMVLD) approach, mixtures of thiol ligands (typically three or more) are combined with *p*-mercaptobenzoic acid (pMBA)-modified gold nanoparticles in one pot to create mixed ligand monolayer/gold nanoparticle conjugates that are rapidly isolated via simple precipitation for subsequent biological screening purposes. SMVLD of our original 120 member conjugate library led to the isolation of conjugates with activity toward *Escherichia coli* growth inhibition comparable to many commercial small-molecule antibiotics.

Herein, we present the results of a nanoscale structure–activity relationship (NSAR) study that has revealed a second antibiotic conjugate with potent activity against several MDR strains of Gram-negative bacteria. The study also uncovered ligand-dependent reductions in the acquisition of resistance by *E. coli* in comparison to a standard small-molecule antibiotic. In addition, the results of a mode of action study are described,

Received: August 16, 2013

   dx.doi.org/10.1021/ja408505n | J. Am. Chem. Soc. XXXX, XXX, XXX–XXX

which indicate that these nanoparticle conjugates are not generally cytotoxic, nonspecific cell membrane disruptors but instead affect the transcription of a number of genes including those involved in conveying multidrug resistance, drug efflux, and cell division. Finally, the biodistribution, clearance, and toxicity of a gold nanoparticle antibiotic was measured in vivo. The results demonstrate that these conjugates can be formulated to be long-circulating and biocompatible agents. Combined with our recent results showing that gold nanoparticles can be formulated to be absorbed efficiently in the gastrointestinal tract (GI) following oral administration,[15] these results support the notion that gold nanoparticles could potentially serve as a new class of orally bioavailable antibiotics for Gram-negative bacteria.

RESULTS AND DISCUSSION

The utility of the SMVLD approach was demonstrated in our laboratories previously by using a set of 10 commercially available thiols to assemble a pilot library of 120 distinct ~2.0 nm diameter gold particle conjugates (Figure 1, compounds **1**–**10**).[5] Several different nanoparticle formulations in the library were found to be potent growth inhibitors of the Gram-negative bacterium *E. coli* (LAL −32, −33, −42; Table 1). (The starting pMBA-capped nanoparticles had no inhibitory activity at the highest concentration tested, 50 μM.) The most potent formulation, LAL-32, contains a core diameter of 2.4 ± 0.6 nm (Supporting Information) and an estimated average mixed monolayer composition of 11 *p*-mercaptobenzoic acids, 33 glutathiones (**5**), 28 cysteamines (**6**), and 15 3-mercapto-1-propanesulfonic acids (**8**) and inhibited bacterial growth by 99.9% as compared to untreated bacteria at a concentration of 250 nM.[5] Conjugation of pMBA and ligands **6**, **8**, and **9** to LAL-33 and LAL-42 was confirmed by solid-state NMR spectroscopy (Supporting Information). In addition to ligand-dependent bacterial growth inhibition, we observed that the ligands must be displayed on the nanoparticle surface to be active.[5] When used as individual free thiols, the 99.9% inhibition concentrations ($IC_{99.9}$) of thiols **6** and **9** were 2 and 0.4 mM, respectively, while the $IC_{99.9}$ values of thiols **5** and **8** were >2 mM. (We define the $IC_{99.9}$ as the minimum concentration necessary to inhibit bacterial growth by 99.9% as determined by plating and colony count analysis. We use IC instead of the more commonly reported MIC because the designation MIC is specific to values determined using visual "turbidity" assays rather than plating. IC equates to MIC but was used here to avoid potential ambiguity in turbidity assays caused by the absorption of nanoparticles.) Combinations of ligands in solution showed no synergy. To quantify this effect, we define the ligand display index (LDI) as the ratio of the $IC_{99.9}$ of a mixture of the free ligands to the $IC_{99.9}$ of the ligands bound to the nanoparticle. The LDI of LAL-32 is ~360, indicating that on a per ligand basis nanoparticles modified with ligands **5**, **6**, and **8** are 360 times more active than the corresponding free ligands.[16]

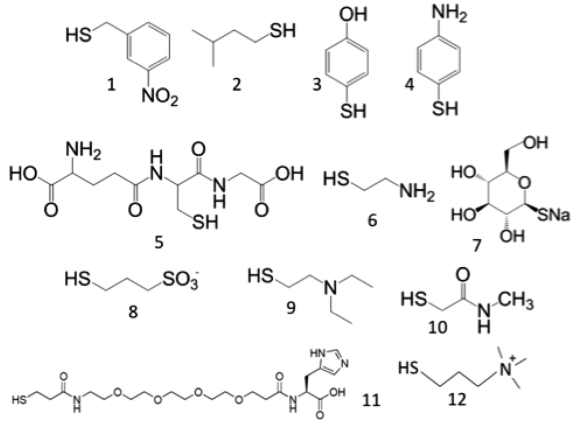

Figure 1. Thiols used in the search for mixed ligand monolayer/gold nanoparticle antibiotic conjugates.

Table 1. List of Gold Nanoparticle Conjugates and $IC_{99.9}$ Values for the Inhibition of *E. coli* (ATCC 25922)

conjugate ID	thiol A	thiol B	thiol C	$IC_{99.9}$ (μM)
LAL-32	**5**	**6**	**8**	0.25
LAL-33	**6**	**8**	9	0.5
LAL-42	**6**	**8**		0.5
LAL-52	**5**	**6**	**11**	0.25

It was then of interest to establish any relationships that might exist between ligand composition and antibiotic activity. We first considered the overlapping ligand set of LAL-32, -33, and -42, which have thiols **6** and **8** in common, and addressed the question of whether the ligand library could be expanded around these thiols to perhaps identify even more potent conjugates. This was accomplished by combining **5**, **6**, and **8** with five new thiols including **11** and **12** in Figure 1. While this expanded search did not yield a more potent conjugate, we did discover an additional nanoparticle formulation that is equipotent to LAL-32 (designated LAL-52, Table 1). This new nanoparticle formulation contains pMBA, glutathione (**5**), cysteamine (**6**), and thiolated histidine (**11**) and inhibited *E. coli* growth with an $IC_{99.9}$ of 250 nM.

The second parameter we established was the rate at which bacteria acquire resistance to the nanoparticle antibiotics. This was accomplished by performing serial passages of *E. coli* in the presence of sub-inhibitory concentrations of gold nanoparticle conjugates (60% of $IC_{99.9}$) for up to 50 days (~2400 generations). The results showed that the time necessary for *E. coli* to develop resistance (where we arbitrarily set the threshold for "resistance" as an increase in $IC_{99.9}$ to 10 μM) against nanoparticle conjugates was dependent upon the mixed thiol monolayer (Figure 2). The shortest time to develop resistance was only 4 days for LAL-42. Other conjugates, however, showed marked delays in the onset of resistance. LAL-52 was not resistance-compromised until 30 days of

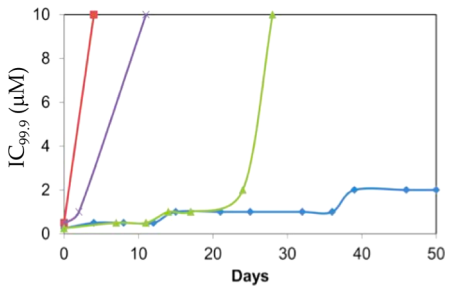

Figure 2. Evolution of resistance of *E. coli* to nanoparticle conjugates: (■) LAL-42, (×) LAL-33, (▲) LAL-52, (◆) LAL-32. Each 10 μM point represents the highest concentration tested, and the $IC_{99.9}$ was not reached.

dx.doi.org/10.1021/ja408505n | J. Am. Chem. Soc. XXXX, XXX, XXX−XXX

passaging, while LAL-32 remained highly active even after 50 days. As a comparison, the rate at which *E. coli* developed resistance to the commercial small-molecule antibiotic chloramphenicol was measured. In contrast to LAL-32, the $IC_{99.9}$ changed rapidly, increasing from 12 to 90 μM in only 2 days.

One of the benefits associated with SMVLD is that activity of nanoparticle conjugates is dependent on the feed ratios of the thiols utilized in the place-exchange reactions. Therefore, one question that arose is whether resistance-compromised nanoparticle formulations can be reactivated by simply modifying their feed ratios during the ligand-exchange step. For example, the synthesis of LAL-33 is the result of a place-exchange reaction utilizing thiol/gold nanoparticle molar ratios of 33 for thiols **8** and **9** and 46 for thiol **6**. While *E. coli* did become resistance-compromised with this specific formulation after about 10 days, the growth of this resistant *E. coli* strain could still be inhibited ($IC_{99.9}$ = 2 μM) by a nanoparticle conjugate synthesized with higher feed ratios of the same thiol ligands (46:1 of each thiol **6**, **8**, and **9**; designated LAL-3346). Solid-state NMR confirmed that each thiol was conjugated to the nanoparticle surface, and the relative ratios of the thiols changed with the different feed ratios used (e.g., less pMBA and a larger 8:6 ratio for LAL-3346 vs LAL-33; Supporting Information).

With the rising threat of MDR Gram-negative bacteria and the number of resistance mechanisms that MDR bacteria possess, we elected to test two of our nanoparticle formulations against some of the MDR Gram-negative ESKAPE pathogens (*Klebsiella pneumoniae*, *Acinetobacter baumannii*, and *Pseudomonas aeruginosa*), in addition to MDR strains of *E. coli* in order to assess whether a representative nanoparticle formulation was specific to *E. coli* or had broader spectrum activity. To address this question, LAL-32 and LAL-52 were assayed against MDR strains of *P. aeruginosa* (clinical isolates UNC A and UNC B from cystic fibrosis patients), *A. baumannii* (ATCC BAA-1605), a New Delhi metallo-β-lactamase (NDM-1) producing strain of *K. pneumoniae* (ATCC BAA-2146), and two MDR *E. coli* strains (ATCC BAA-199 and BAA-200). Activity was observed for all of the Enterobacteriaceae strains tested; *K. pneumoniae* (IC_{99} of 1.25 μM for LAL-52 and $IC_{99.9}$ of 625 nM for LAL-32) and the MDR *E. coli* strains ($IC_{99.9}$ = 156 nM for both LAL-52 and LAL-32), but no activity was observed against the other strains of bacteria tested. This shows that LAL nanoparticles are not specific to *E. coli* and are not affected by the resistance mechanisms of these MDR strains. LAL-32 and LAL-52 are not, however, broad-spectrum antibiotics, as they were not active against strains of *A. baumannii* and *P. aeruginosa*. As we found previously with LAL-32, LAL-52 had no effect on the Gram-positive bacteria tested in this study (*Staphylococcus aureus*, ATCC 29213, and methicillin-resistant *S. aureus*, ATCC BAA-44).

Several experiments were then performed to assess the mode of action of LAL-32. Recognizing that the ligand set in many of the most potent nanoparticle conjugates to emerge from the initial library contained cationic thiols **6** and **9**, we elected to probe whether the mode of action might involve membrane disruption, which is a typical antibacterial mechanism for many cationic small molecules and peptides. Indirect evidence pointing to the absence of membrane disruption was initially established in our NSAR study. We found that when the quaternary ammonium-terminated thiol **12** was substituted for aminothiol **6** in the LAL-32 exchange reaction, no inhibitory activity was observed for the resulting nanoparticle formulation (particles containing **5**, **8**, and **12**). This suggests that thiol **6** has another role besides perturbing the bacterial membrane. This was verified by performing a BacLight membrane permeability assay with LAL-32. Consistent with the thiol substitution experiment described above, it was found that membrane disruption did not occur with LAL-32 against all of the aforementioned bacterial strains.

In an attempt to further delineate the mode of action of LAL-32, we turned to transmission electron microscopy (TEM) to determine whether LAL-32 is able to reach intracellular targets in *E. coli*. After 1 h, LAL-32 nanoparticles were observed to be associated with the outer membrane, and in 6 h, LAL-32 was found deep within the cell (Supporting Information). LAL-32 thus appears to be capable of being internalized into *E. coli*.

Having established that LAL-32 is internalized into *E. coli*, we performed gene expression profiling experiments to determine which pathways LAL-32 might be affecting. Gene expression was compared in *E. coli* incubated with pMBA-Au, LAL-32, and untreated cells. The experiments discovered 154 genes that were differentially expressed upon exposure to LAL-32 (Supporting Information). In general, up-regulation of genes that code for metabolic pathway components, efflux pumps (*emrK*), and membrane proteins was observed in cells treated by LAL-32 and pMBA-Au versus untreated cells. Many of these pathways have been identified as being responsible for multidrug resistance in bacterial systems when treated with other antibiotics. Of particular note is the up-regulation of the multiple antibiotic resistance genes (*mar*). The *mar* gene products confer resistance to a number of structurally unrelated small-molecule drugs such as chloramphenicol, fluoroquinolones, and tetracycline via increased production of efflux pumps. However, this response does not abrogate the growth effects of LAL-32, indicating that intrinsic defense mechanisms of susceptible bacteria are not adequate in counteracting the effects of the nanoparticle.

The down-regulation of transcriptional regulators such as DicC in response to LAL-32 versus pMBA-Au was also noted. DicC is involved in the control of cell division, including activation of the Min family of proteins that regulate the location of FtsZ polymerization. This suggests that LAL-32 may compromise proper formation of the Z-ring during cell division.

Finally, we examined the possibility that gold nanoparticle antibiotics could be used in vivo. The selectivity of the active nanoparticle conjugates for bacterial cells versus mammalian cells was determined first by conducting blood hemolysis assays on defibrinated sheep's blood cells. Within experimental error (~10%), no hemolysis was observed for LAL-33, LAL-42, and LAL-52 even at the highest concentration tested, 50 μM. Nonlinear regression of the hemolysis versus nanoparticle concentration plot for LAL-3346 yielded a relative EC_{50} of 5.6 μM (range of 1.8−18 μM at the 95% confidence limit; Supporting Information). All four nanoparticle conjugates tested were thus highly selective for *E. coli* growth inhibition over hemolysis. MTT toxicity assays were also conducted on Hep G2/2.2.1 cells incubated with LAL-32 and LAL-52 to determine if nanoparticle conjugates interfere with cell proliferation. No toxicity was observed up to concentrations of 0.8 μM, and <40% toxicity was found at the highest concentrations tested, 50 μM. These studies provided some confidence that the LAL nanoparticles could be nontoxic in vivo, prompting us to perform a preliminary murine toxicology study.

dx.doi.org/10.1021/ja408505n | J. Am. Chem. Soc. XXXX, XXX, XXX−XXX

Experiments on gold nanoparticles performed by our laboratories and others have shown that in vivo biodistribution, clearance, and toxicity of ligand-modified gold nanoparticles depend upon the ligand displayed on the gold surface. For instance, the Cliffel lab has shown that tiopronin-modified gold nanoparticles administered via intraperitoneal (i.p.) injection cause renal complications and morbidity,[7] while we have found that glutathione-modified gold nanoparticles are cleared primarily through the renal system without causing any toxicity or morbidity.[15,17] Our initial studies of LAL-32 nanoparticles showed behavior similar to glutathione-modified gold nanoparticles at the lower concentrations administered (10 μM, 200 μL injections). However, similar to tiopronin, renal complications were observed at higher concentrations (60 μM). We have obviated this problem by incorporating a small amount of a thiolated oligoethyleneglycol into the monolayer, with the resulting nanoparticles (LAL-32EG) showing no in vivo toxicity at 60 μM while maintaining an in vitro $IC_{99.9}$ identical to that of the parent LAL-32 particles. Figure 3 shows the blood and urine concentrations for LAL-32EG following a 200 μL i.p. injection of a 60 μM LAL-32EG solution. The particles were cleared primarily through the kidneys, and nanoparticles were found in all major organs examined (heart, liver, spleen, kidneys, lungs; Supporting Information). Although Student's *t* test revealed that the gold concentrations in blood from 1 to 24 h were only statistically different at the 50% confidence limit, a blood circulation half-life was estimated to be 7 ± 3 h using a first-order kinetics model. Combined with our recent results demonstrating that PEG dramatically enhances the absorption of gold nanoparticles in the GI tract,[15] these data suggest that mixed thiol monolayer/gold nanoparticle conjugates may potentially be a viable new platform for orally bioavailable antibiotics.

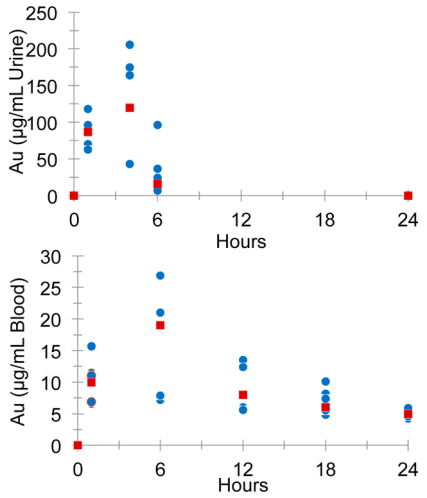

Figure 3. Mass of gold detected in blood and urine following a single 200 μL i.p. injection of 60 μM LAL-32EG nanoparticles. Circles and squares represent individual data points and average, respectively. The points at 0 h report the amounts of gold detected prior to nanoparticle administration.

CONCLUSIONS

The results presented here show that the mixed thiol monolayer/gold nanoparticle conjugates isolated via the SMVLD screening method are potent antibacterial agents against multiple MDR strains of the Gram-negative bacteria *E. coli* and *K. pneumoniae*. Importantly, the conjugates are not generally cytotoxic, nonspecific cell membrane disruptors. They are therefore not "nuisance compounds" that frequently emerge from whole-cell small-molecule drug screens, which act equally on both bacterial and mammalian cells.[18] A preliminary NSAR study was telling in regard to the function of these conjugates, once again revealing the importance of displaying a specific ligand set on the nanoparticle surface. For instance, while conjugates containing **5** and **6** were relatively inactive (90% inhibition at 0.5 μM), the addition of **8** or **11** to **5** and **6** resulted in highly active conjugates (99.9% inhibition at 250 nM). The role of ligands **8** and **11** is not yet clear, but since they have opposite charge, the origin of their activities may involve the ability of both the imidazole and sulfonate moieties to act as H-bond donor/acceptors.

It was also discovered that these gold nanoparticle conjugates exhibited significantly delayed evolution of resistance compared to the small-molecule antibiotic chloramphenicol. Moreover, different resistance rates were observed for nanoparticles with seemingly subtle differences in ligand composition. LAL-32 and LAL-42, for instance, differed by only the deletion of thiol **5** from LAL-32 to LAL-42. Despite having similar initial $IC_{99.9}$ values, however, the rate at which resistance developed changed from >50 days for LAL-32 to 4 days for LAL-42.

A detailed genetic screen revealed that *E. coli* responds to pMBA-Au and LAL-32 by up- or down-regulating many genes. This includes genes involved in the production of multidrug efflux pumps. This appears to have little bearing on the function of LAL-32, however, possibly due to its increased size compared to most small-molecule drugs. Expression of *dicC*, a gene involved in the formation of the Z-ring in its proper position within the dividing cell, was found to be down-regulated. This suggests that LAL-32 may inhibit *E. coli* growth by preventing FtsZ from assembling in its proper location within the cell. Experiments are now underway to test this preliminary hypothesis. Irrespective of the specific mode of action, the low $IC_{99.9}$, low mammalian cell toxicity, and slow onset of resistance observed for these gold nanoparticles suggest that they are potentially viable new candidates for the treatment of MDR Gram-negative bacteria.

METHODS

Synthesis of Gold Nanoparticles. *p*-Mercaptobenzoic acid-capped gold nanoparticles (pMBA Au) were synthesized as previously described. First, 0.4 mmol $HAuCl_4 \cdot 3H_2O$ (Sigma-Aldrich) was dissolved in 20 mL of methanol and stirred at room temperature. Then, 1.36 mmol of pMBA (ITC) was dissolved in 15.5 mL of ultrapure H_2O and 0.6 mL of 10 M NaOH. The pMBA solution was then added to the methanol/gold solution, allowed to stir, and covered with parafilm at room temperature for 24 h. The clear, yellow solution was then divided equally between three 500 mL Erlenmeyer flasks and stirred. To each flask we added 62 mL of methanol followed by 178 mL of ultrapure H_2O. $NaBH_4$ was then hydrated and added to each flask immediately (2.4 mL of 0.25 M per flask). Twenty-four milliliters of ultrapure H_2O was then added to each flask. The solutions were allowed to stir at room temperature overnight. Gold nanoparticles were precipitated by adding 2 mL of 5 M NaCl and 150 mL of ultrapure H_2O to each flask and pelleted at 3200*g* for 5 min. After being dried overnight, the particles were resuspended in filter-sterilized (0.22 μm) ultrapure H_2O. Particle concentration was determined via UV−visible spectroscopy (ε_{510nm} = 409 440 M^{-1} cm^{-1}). Further, it was noted that the source of reagents for this synthesis is important to the preparation. Ensuring that reagents were not stored with other chemicals that could react or contaminate them was also critical.

dx.doi.org/10.1021/ja408505n | J. Am. Chem. Soc. XXXX, XXX, XXX−XXX

Transmission electron microscopy and PAGE were used to determine the average size and purity of the particles (Figures S1 and S2).

Place-Exchange Reactions. One-pot place-exchange reactions were conducted with 7.4 μM gold nanoparticles in 4 mL of 20 mM pH 9.5 sodium phosphate buffer. Feed ratios of thiols were as follows: thiols **5**, **8**, and **9** were utilized in 33× molar excess of gold nanoparticles, while thiols **6** and **12** were utilized at 46× molar excess of gold nanoparticles. Thiol **11** was utilized in 18× molar excess of gold. These ratios were adopted for this study following an extensive NSAR study in which a range of feed ratios was tested in order to optimize nanoparticle activity. Stocks of thiols were 20 mM in water, except for thiol **11**, which was dissolved in DMSO. Reactions were placed on a plate shaker and agitated for 24 h at 19 °C. The exchange product was harvested through the addition of 2 mL of 5 M NaCl and 9 mL of methanol. Reactions were centrifuged at 3200*g* for 20 min, and the supernatant was then discarded. The nanoparticle pellet was resuspended in ∼500 μL filter-sterilized ultrapure H_2O and precipitated again with the addition of 500 μL of 5 M NaCl and 8 mL of methanol and pelleted at 3200*g* for 10 min. The supernatant was discarded, and the particles were allowed to dry to completion overnight at room temperature and resuspended in filter-sterilized ultrapure water and washed over a 10K MWCO centricon filter to remove excess salt and thiol (8 × 4 min at 12 000*g*). TEM was used to determine the size of the exchange product LAL-32 (Supporting Information). The size distribution was observed to increase slightly (Supporting Information), with particles ranging in size from ∼1.3 to 2.7 nm (size standard deviation of 0.4 nm vs 0.2 nm for pMBA-Au). As the molar extinction coefficient for gold nanoparticles in this size regime does not change considerably (2.33×10^5 and 1.29×10^6 M^{-1} cm^{-1} for 1.3 and 2.7 nm diameter gold nanoparticles, respectively),[19] the extinction coefficient reported above for 2.2 nm diameter particles was used to prepare solutions of LAL-32 for bacterial growth inhibition assays. UV−visible spectroscopy (Supporting Information) confirmed that the major product in the synthesis of LAL-32 consisted of particles with similar visible light extinction characteristics to the starting pMBA-Au nanoparticles.

Nanoparticle Characterization by NMR. Solid-state, cross-polarization magic angle spinning (CPMAS) ^{13}C NMR was used to verify the ligands on the gold surface and to estimate the distribution of the individual ligands on the gold surface. NMR was performed using a Varian INOVA-400 (Agilent Technologies, Inc.) spectrometer operating at 100.63 MHz for ^{13}C observation. For more details on spectral acquisition and optimization, see Supporting Information.

Bacterial Growth Inhibition Assays. Inoculation of *E. coli* into 3 mL of Mueller−Hinton broth (Fisher) was carried out by touching the top of four well-isolated colonies of *E. coli* (ATCC 25922) from a Mueller−Hinton agar (Fisher) plate with an inoculation loop. The culture was allowed to grow at 37 °C, 225 rpm, for 4 h after which it was diluted to 1×10^6 CFU/mL in Mueller−Hinton broth. Equal volumes of diluted inoculum and nanoparticle sample (adjusted to the correct assay concentration in Mueller−Hinton broth) were mixed to make the final inoculum concentration 5×10^5 CFU/mL. Samples were incubated at 37 °C, 225 rpm, for 18 h. End points were determined by colony counting on Mueller−Hinton agar after dilution of each sample in PBS and incubation of the plates at 37 °C for 24 h. Growth inhibition assays for *K. pneumoniae* were performed by performing broth microdilution in cation-adjusted Mueller hinton broth as previously reported,[20] then plating colonies on nutrient agar and enumerating.

Resistance Assays. *E. coli* cells were passed up to 50 days in broth containing 60% of the $IC_{99.9}$ value of nanoparticle conjugates. Minimal inhibitory concentration screening at various time points occurred in order to monitor the $IC_{99.9}$ of various nanoparticle compounds. Resistance of *E. coli* to nanoparticle conjugates was defined as an increase in $IC_{99.9}$ to 10 μM.

Hemolysis Assays. Assays were performed on mechanically defibrinated sheep blood (Hemostat Laboratories: DSB100). Approximately 1 mL of blood was placed into a microcentrifuge tube and centrifuged at 10 000*g* for 10 min. The supernatant was removed, and then the cells were resuspended with 1 mL of phosphate-buffered saline (PBS). The suspension was centrifuged, the supernatant was removed, and cells were resuspended two more times. Test compounds were diluted in 1× PBS, and 10 μL of washed cells was added to a range of compound concentrations (total volume was 100 μL). Cells incubated in only PBS were used as a negative control and as a zero hemolysis marker, whereas a 0.1% Triton X sample was used as a positive control and a 100% lysis marker. Samples were then placed in an incubator at 37 °C, 225 rpm, for 24 h. After incubation, remaining cells were pelleted by centrifugation at 3220*g* for 5 min and washed with 100 μL of 1× PBS three times. Finally, the cells were diluted 1:10 in 1× PBS and lysed with the addition of 0.1% Triton X. Absorbance at 414 nm was measured to determine the amount of heme released from cell lysis after they survived the incubation with test compounds.

Cell Culture. HepG2/2.2.1 liver cells (ATCC CRL-11997) were cultured in DMEM supplemented with 10% FBS and 1% penicillin/strepavidin at 37 °C with 5% CO_2. The medium was changed to calcium and magnesium-free 1× D-PBS with 10% FBS for all nanoparticle assays.

MTT Assays. Cell viability assays were conducted using an MTT kit (Biotium #30006) as indicated by manufacturer's instructions. Briefly, cells were seeded at 2.5×10^5 cells/well in 96-well plates in 1× D-PBS with 10% FBS. After 30 min, test compounds were added to the cells and incubated at 37 °C and 5% CO_2 for 24 h. Cells in media only were used as a negative control and 100% survival, whereas 0.1% Triton X was added to cells as a positive control and 0% survival. After the 24 h incubation, cells were washed two times with 1× D-PBS to remove excess nanoparticles, and 100 μL of DMEM was added to the surviving cells. Ten microliters of MTT reagent was added to each well, and the cells were incubated at 37 °C, in 5% CO_2, for 4 h. Finally, 200 μL of DMSO was added to the media to dissolve the formazan salt product. Absorbance measurements at 595 nm were acquired, and percent survival was determined.

Membrane Permeability Assay. The BacLight assay (Invitrogen) was used to assess membrane permeability. Bacteria were grown overnight in cation-adjusted Mueller−Hinton broth at 37 °C with shaking. The culture was diluted 1:40 in broth and grown to an optical density at 600 nm of ∼1.0 (∼4 h growth). The cultures were centrifuged at 10 000*g* for 15 min, and the cell pellet was washed once in sterile water, with a subsequent resuspension at 1/10th of the original volume. Further dilution to 1:20 into water with test compound then occurred. Suspensions were incubated at 37 °C with shaking for 1 h. Samples were then centrifuged at 10 000*g* for 10 min, washed once with sterile water, and resuspended in water. A 1:1 mixture of SYTO-9 and propidium iodide (3 μL/mL) was added to the suspension and mixed well. One hundred microliters of the suspension was then added to each well of a 96-well plate, and the plates were incubated in the dark for 15 min at room temperature. Green fluorescence (SYTO-9) was read at 530 nm, and the red fluorescence (propidium iodide) was read at 645 nm (excitation wavelength 485 nm). The ratio of green to red fluorescence was expressed as a percentage of the control.

TEM. *E. coli* was cultured in Mueller−Hinton broth media (Becton, Dickinson and Company) and adjusted to an optical density of 1 at 600 nm. LAL-32 nanoparticle conjugates were added to a bacterial solution of OD_{600} = 1 at a concentration of 2 μM. After 1 or 6 h, the mixture of bacteria and LAL-32 was centrifuged at 12 000 rpm for 15 min. The bacterial cell pellets were resuspended with 1× PBS and centrifuged to remove excess LB broth medium. The cell pellets were then fixed with 2.5% glutaraldehyde (Electron Microscope Sciences) in 0.1 M sodium cacodylate (Electron Microscope Sciences) buffer overnight at 4 °C and postfixed with 1% osmium tetraoxide (Electron Microscope Sciences) in 0.1 M sodium cacodylate buffer for 2 h at room temperature. After being washed with cacodylate buffer, cell pellets were dehydrated with progressive concentrations of ethanol as follows: 70, 80, 90, 95, and 100% for 10 min each and 100% acetone twice for 10 min. The cell pellets were infiltrated using a mixture of propylene oxide to Spurr's resin at 1:2, 1:1, and 2:1 volume ratios for 1 h each and 100% resin overnight. The cell pellets were finally embedded in resin at 60 °C for 24−48 h. Ultrathin sections (60−70

dx.doi.org/10.1021/ja408505n | J. Am. Chem. Soc. XXXX, XXX, XXX−XXX

nm thickness) were cut using Leica UC6 Ultramicrotome. The sections were collected onto 300 mesh copper grids (Electron Microscope Sciences) and stained with 2% uranyl acetate (Electron Microscope Sciences) and 1% lead citrate (Electron Microscope Sciences) solutions. TEM imaging and analysis were conducted using a Philips CM100 microscope with an 80 kV acceleration voltage.

Animal Protocols. Animals were housed at the Keck Facility, a University of Colorado Division of Animal Care (DAC) facility, fully certified by the Association for Assessment and Accreditation of Laboratory Animal Care (AAALAC). Animals were housed under the full supervision of the full-time veterinarian and staff. All procedures performed were previously approved by the University of Colorado's Institutional Animal Care and Use Committee (IACUC). Balb/c, 5−6 week, 15−16 g, female mice were purchased from Harlan Laboratories. Nanoparticle formulations were prepared in DPBS (n = 15 mice per concentration of LAL-32; n = 25 mice per concentration for LAL-32EG). A 10 or 60 μM concentration in 200 μL volume of each nanoparticle formulation was administered to individual mice by intraperitoneal injection. Blood was drawn via submandibular bleeding techniques in compliance with our protocol and bleeding guidelines for mL/kg body weight per week. Urine was collected on cellophane with precautions taken to avoid fecal contamination. Mice were euthanized at 24 h, 2 weeks, 4 weeks, 8 weeks, and 12 weeks by carbon dioxide asphyxiaation followed by cervical dislocation. Five mice were sampled from each group for biodistribution analysis. Blood, urine, and tissue samples were prepared as described in Simpson et al. with no modifications or exceptions.[7]

Analysis of gold content in biological samples was performed using a Perkin-Elmer SCIEX ICP-MS (model #Elan DRC-e, Vernon Hills, Illinois) at the University of Colorado Laboratory for Environmental and Geological Sciences (LEGS). Statistical analysis of samples was performed as described in Simpson et al. with no exceptions.[7] The detection limit of the instrument was 0.02 ppb or 0.02 ng Au/mL sample.

Gene Expression Profiling. A 4 mL overnight culture of *E. coli* (ATCC 25922) was diluted into 75 mL Mueller−Hinton broth and grown to OD_{600} = 0.7. The bacterial culture was then divided equally into eight 4 mL cultures. Nanoparticle conjugates LAL-32 (in triplicate) and pMBA-Au (in duplicate) were added to a final concentration of 2.5 μM. Bacteria only (containing no nanoparticle conjugate) controls were performed in triplicate. The incubations took place at 37 °C and 225 rpm for 2 h followed by centrifugation at 3200g for 5 min. The cell pellets were frozen overnight and mailed (on ice) to GenUs Biosystems (Northbrook, IL) for total RNA harvest and microarray anaylsis using an Agilent *E. coli* 8x15K array. Data analysis was performed by GenUS Biosystems using Agilent Feature Extraction and GeneSpring GX software packages

■ ASSOCIATED CONTENT

Supporting Information

Additional figures and tables and discussed in the article. This material is available free of charge via the Internet at http://pubs.acs.org.

■ AUTHOR INFORMATION

Corresponding Authors

ccmeland@ncsu.edu
daniel.feldheim@colorado.edu

Notes

The authors declare no competing financial interest.

■ ACKNOWLEDGMENTS

The authors would like to thank generous support from The Bill and Melinda Gates Foundation.

■ REFERENCES

(1) http://www.foxbusiness.com/personal-finance/2011/04/08/antibiotics-siege-groups-action/.

(2) Spellberg, B.; Guidos, R.; Gilbert, D.; Bradley, J.; Boucher, H. W.; Scheld, W. M.; Bartlett, J. G.; Edwards, J. *Clin. Infect. Dis.* **2008**, *46*, 155−164.

(3) Bowman, M. C.; Ballard, T. E.; Ackerson, C. J.; Feldheim, D. L.; Margolis, D. M.; Melander, C. *J. Am. Chem. Soc.* **2008**, *130*, 6896−6897.

(4) Bresee, J.; Maier, K. E.; Boncella, A. E.; Melander, C.; Feldheim, D. L. *Small* **2011**, *7*, 2027−2031.

(5) Bresee, J.; Maier, K. E.; Melander, C.; Feldheim, D. L. *Chemical Communications* **2013**, *46*, 7516−7518. Note: The absolute number of each ligand/nanoparticle was estimated based upon a chemical formula for the pMBA-capped gold nanoparticle starting material, which had a diameter (2.2 ± 0.4 nm) (Supporting Information) similar to particles characterized by mass spectrometry as $Au_{230}L_{87}$. See: Wong, A. O.; Heinecke, C. L.; Simone, A. R.; Whetten, R. L.; Ackerson, C. J. *Nanoscale* **2012**, *4*, 4099. Average percentage values for the ligands on LAL-32 were determined previously as 13% *p*-MBA, 38% **5**, 32% **6**, and 17% **8**. While some broadening of the nanoparticle diameter was observed following ligand exchange (LAL-32 diameter = 2.4 ± 0.6 nm; Supporting Information), these percentages, and an average of 87 ligands/particle, were used to estimate absolute values for ligand coverage.

(6) Zhao, Y. Y.; Tian, Y.; Cui, Y.; Liu, W. W.; Ma, W. S.; Jiang, X. Y. *J. Am. Chem. Soc.* **2010**, *132*, 12349−12356.

(7) Simpson, C. A.; Huffman, B. J.; Gerdon, A. E.; Cliffel, D. E. *Chem. Res. Toxicol.* **2010**, *23*, 1608−1616.

(8) Fischer, N. O.; McIntosh, C. M.; Simard, J. M.; Rotello, V. M. *Proc. Natl. Acad. Sci. U.S.A.* **2002**, *99*, 5018−5023.

(9) De, M.; You, C. C.; Srivastava, S.; Rotello, V. M. *J. Am. Chem. Soc.* **2007**, *129*, 10747−10753.

(10) Boal, A. K.; Rotello, V. M. *J. Am. Chem. Soc.* **2000**, *122*, 734−735.

(11) Tshikhudo, T. R.; Wang, Z.; Brust, M. *Mater. Sci. Technol.* **2004**, *20*, 980−984.

(12) Hostetler, M. J.; Templeton, A. C.; Murray, R. W. *Langmuir* **1999**, *15*, 3782−3789.

(13) Chen, S.; Templeton, A. C.; Murray, R. W. *Langmuir* **2000**, *16*, 3543−3548.

(14) Brust, M.; Walker, M.; Bethell, D.; Schiffrin, D. J.; Whyman, R. *Chem. Commun.* **1994**, 801−802.

(15) Smith, C.; Kim, C. A. S.; Carter, C. J.; Feldheim, D. L. *ACS Nano* **2013**, *7*, 3991.

(16) LDI is the $IC_{99.9}$ of a mixture of the free ligands divided by the $IC_{99.9}$ of those same ligands bound to the nanoparticle. The $IC_{99.9}$ of the free ligands was 8 mM. The $IC_{99.9}$ of the ligands bound to the nanoparticles was 22 μM, which is the $IC_{99.9}$ of the nanoparticles (250 nM) multiplied by the estimated value of 87 ligands/particle.

(17) Simpson, C. A.; Salleng, K. J.; Cliffel, D. E.; Feldheim, D. L. *Nanomedicine* **2013**, *9*, 257−263.

(18) Payne, D. J.; Gwynn, M. N.; Holmes, D. J.; Pompliano, D. L. *Nat. Rev. Drug Discovery* **2007**, *6*, 29−40.

(19) Rance, G. A.; Marsh, D. H.; Khlobystov, A. N. *Chem. Phys. Lett.* **2008**, *460*, 230−236.

(20) Worthington, R. J.; Bunders, C. A.; Reed, C. S.; Melander, C. *ACS Med. Chem. Lett.* **2012**, *3*, 357−361.